Research Article Vol. 31, No. 6 / 13 Mar 2023 / Optics Express 9996
Optics EXPRESS

Morphology-dependent resonance induced optical forces in a multiple-sphere system

HUANHUAN WANG,[1] ZHENYU HAN,[1] LEI ZHANG,[2,3] AND JUN CHEN[1,3,*]

[1]State Key Laboratory of Quantum Optics and Quantum Optics Devices, Institute of Theoretical Physics, Shanxi University, Taiyuan 030006, China
[2]State Key Laboratory of Quantum Optics and Quantum Optics Devices, Institute of Laser Spectroscopy, Shanxi University, Taiyuan 030006, China
[3]Collaborative Innovation Center of Extreme Optics, Shanxi University, Taiyuan 030006, China
*chenjun@sxu.edu.cn

Abstract: Optical fields and forces can be greatly enhanced for a microparticle when the whispering gallery modes (WGMs) are excited. In this paper, by solving the scattering problem using the generalized Mie theory, the morphology-dependent resonances (MDRs) and resonant optical forces derived from the coherent coupling of WGMs are investigated in multiple-sphere systems. When the spheres approach each other, the bonding and antibonding modes of MDRs emerge and correspond to the attractive and repulsive forces, respectively. More importantly, the antibonding mode is good at propagating light forward, while the optical fields decay rapidly for the bonding mode. Moreover, the bonding and antibonding modes of MDRs in the PT-symmetric system can persist only when the imaginary part of the refractive index is small enough. Interestingly, it is also shown that for a PT-symmetric structure, only a minor imaginary part of the refractive index is required to generate a significant pulling force at MDRs, making the whole structure move against the light propagation direction. Our work deepens the understanding of the collective resonance behavior of multiple spheres and paves the way for potential applications in particle transportation, non-Hermitian systems, integrated optical devices, etc.

1. Introduction

Confining light at the nanoscale has attracted widespread interest due to its numerous applications [1–3]. A nanoscale whispering gallery modes (WGMs) particle is considered an important tool in light confining and enhancement due to its high quality (Q) factor [4]. Similar to the reflection of sound waves on walls, the optical WGMs exist at the curved interface of high refractive index materials [5,6]. In 1908, Mie theoretically studied the WGMs in a spherical cavity indirectly through scattering spectroscopy [7]. In 1977, Ashkin and Dziedzic first observed the enhancement of the radiation pressure induced by WGMs [8]. Subsequently, the resonance peak corresponding to WGMs observed in fluorescence spectra also attracted wide attention [9]. Various high-Q WGMs optical microcavities have been studied, such as high-sensitivity sensors, low-threshold lasers, etc. [10–15]. Moreover, the optical forces and resonances in two-sphere systems are also explored [16–20]. In reality, a system usually has multiple particles, such as optical matter [21,22]. Thus, it is important to know the morphology-dependent resonances (MDRs) and the resonant optical forces' behavior in multiple-sphere systems.

The concept of PT-symmetry was first introduced into quantum mechanics by Bender in 1998 [23,24], and it has triggered many new and interesting phenomena in other fields [25–31]. In optics, PT-symmetry can be established by incorporating gain and loss with the refractive index satisfying $n(\mathbf{r}) = n^*(-\mathbf{r})$ [32–34]. Many applications such as optical switches and lasers have been discovered [35–38], and studies on optical forces in PT-symmetric systems are also carried

#484436 https://doi.org/10.1364/OE.484436
Journal © 2023 Received 27 Dec 2022; revised 6 Feb 2023; accepted 20 Feb 2023; published 3 Mar 2023

Optics EXPRESS

out [39,40]. Then the natural question is: how do MDRs and their induced optical forces behave in PT-symmetric systems?

This paper systematically investigates the resonant behavior and resonant optical forces induced by MDRs in multiple-sphere systems. Unique resonance phenomena in multiple-sphere systems are exhibited, and the interesting pulling effect of optical forces generated by MDRs in PT-symmetric systems is found. This work dramatically extends the previous studies on MDRs and adds more degrees of freedom for optical micromanipulation.

2. Optical force acting on each sphere in a multiple-sphere system

The time-averaged optical force acting on a sphere (e. g. sphere j, for simplicity, dropping the sphere index j) in a multiple-sphere system illuminated by an arbitrary incident optical field can be calculated by integrating the Maxwell stress tensor over the outer surface of the sphere [41,42]

$$\langle \mathbf{F} \rangle = \oiint_S \mathbf{n} \cdot \langle \mathbf{T} \rangle d\sigma, \tag{1}$$

in which $\mathbf{n}$ and $d\sigma$ are the local outward unit normal and the area element of the surface S, respectively. The time-averaged Maxwell stress tensor is given by

$$\langle \mathbf{T} \rangle = \frac{1}{2}\mathrm{Re}[\varepsilon_0 \mathbf{E}\mathbf{E}^* + \mu_0 \mathbf{H}\mathbf{H}^* - \frac{1}{2}(\varepsilon_0 \mathbf{E}\cdot\mathbf{E}^* + \mu_0 \mathbf{H}\cdot\mathbf{H}^*)\mathbf{I}], \tag{2}$$

where ε_0 (μ_0) is the permittivity (permeability) of the background medium, $\mathbf{I}$ is the unit dyad, $\mathbf{E}\mathbf{E}^* \equiv \mathbf{E}\otimes\mathbf{E}^*$ and $\mathbf{H}\mathbf{H}^* \equiv \mathbf{H}\otimes\mathbf{H}^*$ with $\otimes$ the dyadic product, $\mathbf{E}$ and $\mathbf{H}$ are the total electromagnetic fields surrounding the sphere, i.e., the sum of the incident $\mathbf{E}_i$ ($\mathbf{H}_i$) and the scattered $\mathbf{E}_s$ ($\mathbf{H}_s$) fields that can be expressed in terms of the vector spherical wave functions $\mathbf{M}^{(J)}_{m,n}$, $\mathbf{N}^{(J)}_{m,n}$ [43]

$$\begin{aligned}
\mathbf{E}_i &= -\sum_{n,m} iE_{m,n}[p_{m,n}\mathbf{N}^{(1)}_{m,n}(k,\mathbf{r}) + q_{m,n}\mathbf{M}^{(1)}_{m,n}(k,\mathbf{r})],\\
\mathbf{H}_i &= -\frac{k}{\omega\mu}\sum_{n,m} E_{m,n}[q_{m,n}\mathbf{N}^{(1)}_{m,n}(k,\mathbf{r}) + p_{m,n}\mathbf{M}^{(1)}_{m,n}(k,\mathbf{r})],\\
\mathbf{E}_s &= \sum_{n,m} iE_{m,n}[a_{m,n}\mathbf{N}^{(3)}_{m,n}(k,\mathbf{r}) + b_{m,n}\mathbf{M}^{(3)}_{m,n}(k,\mathbf{r})],\\
\mathbf{H}_s &= \frac{k}{\omega\mu}\sum_{n,m} E_{m,n}[b_{m,n}\mathbf{N}^{(3)}_{mn}(k,\mathbf{r}) + a_{m,n}\mathbf{M}^{(3)}_{mn}(k,\mathbf{r})],
\end{aligned} \tag{3}$$

where

$$E_{m,n} = |E_0| i^n \left[\frac{(2n+1)}{n(n+1)}\frac{(n-m)!}{(n+m)!}\right]^{1/2}, \tag{4}$$

i is the imaginary unit, k is the wave number in the background medium, $\mathbf{r}$ is the position vector in the jth coordinate system with the origin setting at the center of sphere j, n runs from 1 to $+\infty$, including all orders of multipoles, and m from -n to + n in the summation. $p_{m,n}$ and $q_{m,n}$($a_{m,n}$ and $b_{m,n}$) are the partial wave expansion coefficients for incident (scattered) fields, and it follows from the boundary conditions [44] that

$$a_{m,n} = a_n p_{m,n}, \qquad b_{m,n} = b_n q_{m,n}, \tag{5}$$

where a_n and b_n are the Mie coefficients [45]. It should be noted that the incident field $\mathbf{E}_i(\mathbf{H}_i)$ in Eq. (3) striking at the surface of sphere j consists of both the initial incident waves and the scattered fields of all other spheres ($l \neq j$), thus the corresponding expansion coefficients calculated

Optics EXPRESS

by using the multiple scattering theory [46] are

$$\begin{aligned}
p_{m,n} &= p_{m,n}^{(j,j)} + \sum_{l\neq j} p_{m,n}^{(l,j)} = p_{m,n}^{(j,j)} - \sum_{l\neq j}\sum_{\nu,u}[a_{u\nu}^{(l)}A_{m,n}^{u\nu}(l,j) + b_{u\nu}^{(l)}B_{m,n}^{u\nu}(l,j)],\\
q_{m,n} &= q_{m,n}^{(j,j)} + \sum_{l\neq j} q_{m,n}^{(l,j)} = q_{m,n}^{(j,j)} - \sum_{l\neq j}\sum_{\nu,u}[a_{u\nu}^{(l)}B_{m,n}^{u\nu}(l,j) + b_{u\nu}^{(l)}A_{m,n}^{u\nu}(l,j)],\\
a_{m,n} &= a_n\left\{p_{m,n}^{(j,j)} - \sum_{l\neq j}\sum_{\nu,u}[a_{u\nu}^{(l)}A_{m,n}^{u\nu}(l,j) + b_{u\nu}^{(l)}B_{m,n}^{u\nu}(l,j)]\right\},\\
b_{m,n} &= b_n\left\{q_{m,n}^{(j,j)} - \sum_{l\neq j}\sum_{\nu,u}[a_{u\nu}^{(l)}B_{m,n}^{u\nu}(l,j) + b_{u\nu}^{(l)}A_{m,n}^{u\nu}(l,j)]\right\},
\end{aligned} \tag{6}$$

where $p_{m,n}^{(j,j)}(q_{m,n}^{(j,j)})$ and $p_{m,n}^{(l,j)}(q_{m,n}^{(l,j)})$ denote the partial wave expansion coefficients for the initial incident waves exerted on sphere j and the incident waves from the scattering of other spheres ($l\neq j$), respectively, $A_{m,n}^{u\nu}(l,j)$ and $B_{m,n}^{u\nu}(l,j)$ [45,46] are the translation coefficients for the transformation from the origin centered at sphere l to that of sphere j.

So the total external fields in Eq. (2) at the surface of sphere j should be

$$\begin{aligned}
\mathbf{E} &= \sum_{n,m} iE_{m,n}[a_{m,n}\mathbf{N}_{m,n}^{(3)}(k,\mathbf{r}) + b_{m,n}\mathbf{M}_{m,n}^{(3)}(k,\mathbf{r}) - p_{m,n}\mathbf{N}_{m,n}^{(1)}(k,\mathbf{r}) - q_{m,n}\mathbf{M}_{m,n}^{(1)}(k,\mathbf{r})],\\
\mathbf{H} &= \frac{k}{\omega\mu}\sum_{n,m} E_{m,n}[b_{m,n}\mathbf{N}_{m,n}^{(3)}(k,\mathbf{r}) + a_{m,n}\mathbf{M}_{m,n}^{(3)}(k,\mathbf{r}) - q_{m,n}\mathbf{N}_{m,n}^{(1)}(k,\mathbf{r}) - p_{m,n}\mathbf{M}_{m,n}^{(1)}(k,\mathbf{r})].
\end{aligned} \tag{7}$$

When the background medium is lossless, the integration of the Maxwell stress tensor in Eq. (1) can be done over an infinitely large sphere surface instead of at each sphere's outer surface due to the conservation of momentum. Then, after some algebra, the optical force can be expressed in terms of the expansion coefficients of scattering and incident fields [47]

$$F_x = \mathrm{Re}[\mathcal{F}_1], \qquad F_y = \mathrm{Im}[\mathcal{F}_1], \qquad F_z = \mathrm{Re}[\mathcal{F}_2], \tag{8}$$

where

$$\begin{aligned}
\mathcal{F}_1 = \frac{2\pi\varepsilon_0}{k^2}|E_0|^2\sum_{n=1}^{\infty}\sum_{m=-n}^{n}\Bigg\{&\frac{[(n-m)(n+m+1)]^{1/2}}{n(n+1)}(\tilde{a}_{m,n}\tilde{b}_{m+1,n}^{*}+\tilde{b}_{m,n}\tilde{a}_{m+1,n}^{*}-\tilde{p}_{m,n}\tilde{q}_{m+1,n}^{*}-\tilde{q}_{m,n}\tilde{p}_{m+1,n}^{*})\\
&-\left[\frac{n(n+2)(n+m+1)(n+m+2)}{(n+1)^2(2n+1)(2n+3)}\right]^{1/2}(\tilde{a}_{m,n}\tilde{a}_{m+1,n+1}^{*}+\tilde{b}_{m,n}\tilde{b}_{m+1,n+1}^{*}-\tilde{p}_{m,n}\tilde{p}_{m+1,n+1}^{*}-\tilde{q}_{m,n}\tilde{q}_{m+1,n+1}^{*})\\
&+\left[\frac{n(n+2)(n-m)(n-m+1)}{(n+1)^2(2n+1)(2n+3)}\right]^{1/2}(\tilde{a}_{m,n+1}\tilde{a}_{m+1,n}^{*}+\tilde{b}_{m,n+1}\tilde{b}_{m+1,n}^{*}-\tilde{p}_{m,n+1}\tilde{p}_{m+1,n}^{*}-\tilde{q}_{m,n+1}\tilde{q}_{m+1,n}^{*})\Bigg\},
\end{aligned} \tag{9}$$

$$\begin{aligned}
\mathcal{F}_2 = -\frac{4\pi\varepsilon_0}{k^2}|E_0|^2\sum_{n=1}^{\infty}\sum_{m=-n}^{n}\Bigg\{&\frac{m}{n(n+1)}(\tilde{a}_{m,n}\tilde{b}_{m,n}^{*}-\tilde{p}_{m,n}\tilde{q}_{m,n}^{*})\\
&+\left[\frac{n(n+2)(n-m+1)(n+m+1)}{(n+1)^2(2n+1)(2n+3)}\right]^{1/2}(\tilde{a}_{m,n}\tilde{a}_{m,n+1}^{*}+\tilde{b}_{m,n}\tilde{b}_{m,n+1}^{*}-\tilde{p}_{m,n}\tilde{p}_{m,n+1}^{*}-\tilde{q}_{m,n}\tilde{q}_{m,n+1}^{*})\Bigg\},
\end{aligned} \tag{10}$$

and

$$\begin{aligned}
\tilde{a}_{m,n} &= a_{m,n} - \tfrac{1}{2}p_{m,n}, \qquad \tilde{p}_{m,n} = \tfrac{1}{2}p_{m,n},\\
\tilde{b}_{m,n} &= b_{m,n} - \tfrac{1}{2}q_{m,n}, \qquad \tilde{q}_{m,n} = \tfrac{1}{2}q_{m,n}.
\end{aligned} \tag{11}$$

Our calculations are general for arbitrary incident light and are accurate in principle within classical electrodynamics, and the numerical convergence is controlled by the maximum angular

Optics EXPRESS

momentum (set to 65, for the size parameters used here) at which the series expansion was truncated.

In addition, the total optical force exerted on the whole multiple-sphere system is

$$\mathbf{F}_{tot} = \sum_{j=1}^{N} \mathbf{F}_j, \tag{12}$$

where N is the total number of the spheres in the system. Moreover, the optical force of each sphere with respect to the averaged force of the entire particle system is expressed as

$$\mathbf{F}_{rel} = \mathbf{F}_j - \mathbf{F}_{tot}/N, \tag{13}$$

indicating the relative motion of each sphere.

3. Numerical results and discussion

Numerical calculations (conveyed in terms of frequency) are carried out to investigate the resonant optical force in a multiple-sphere system when WGMs are excited and coupled coherently. For simplicity, the multiple-sphere system is composed of a line of spheres (radius $R = 2.5\mu$m) illuminated by a linearly polarized (x-polarized) plane wave propagating along the sphere cluster's axis (z-axis) with a modest intensity of 10^4 W/cm^2.

Due to the high-Q factor, the optical force exerted on a single polystyrene sphere increases visibly when the WGMs are excited, which can be seen from the sharp peak 39TE1 in Fig. 1, and the enhanced electromagnetic fields near the surface of the sphere are shown beside the peak. Moreover, when two spheres approach each other, the optical force enhances more significantly (see the force acting on the first sphere as an example denoted by the red line in Fig. 1). Their WGMs are coherently coupled and split into the bonding and antibonding modes through quasi-normal mode splitting [48,49], similar to the hybridization of atomic orbitals in electronic systems [50]. The resonant frequencies of the bonding and antibonding modes are lower and higher than that of a single sphere. The same rules apply to multiple-sphere systems. As the number of spheres increases (see the configuration denoted by the inset), the resonant frequencies of the splitting antibonding modes will exhibit blueshift. In contrast, there is no consistent trend for resonant frequencies of the bonding modes. However, with the further increase in the number of spheres, the blueshift phenomenon of antibonding modes is no longer obvious, and the peak positions of the bonding and antibonding modes will stabilize due to weakening coupling between the newly added particles and the first sphere. Furthermore, the resonant line widths are much wider than that of a single sphere, providing more robustness against size dispersion in the study of MDRs in experiments. For the system composed of two spheres, the amplitude of the bonding mode is larger than that of the antibonding mode, while for the system composed of multiple spheres, the situation is quite different. We will further illuminate this later. It should be noted that we chose the 39TE1 mode because it is very sharp and far from other modes (peaks) [18]. This can avoid the impact of coupling and splitting of other modes in the multiple-sphere system.

Regardless of the number of spheres in the system, the bonding and antibonding modes all correspond to the attractive and repulsive force, respectively, as can be seen in Fig. 2, in which we plot the optical force exerted on each sphere with respect to the averaged force of the entire particle system [see Eq. (13)]. For the bonding modes indicated by the orange stars, the optical forces tend to make the whole system form a stable structure. For the two-sphere system, the two spheres move towards each other under the action of attractive force, forming a stable structure that moves together [see Fig. 2(a)]. While for the system composed of three or four spheres, the first sphere moves upwards, and the other spheres move downwards, thus also forming a stable structure [see Figs. 2(b) and 2(c)]. As the number of spheres further increases, as shown

Optics EXPRESS

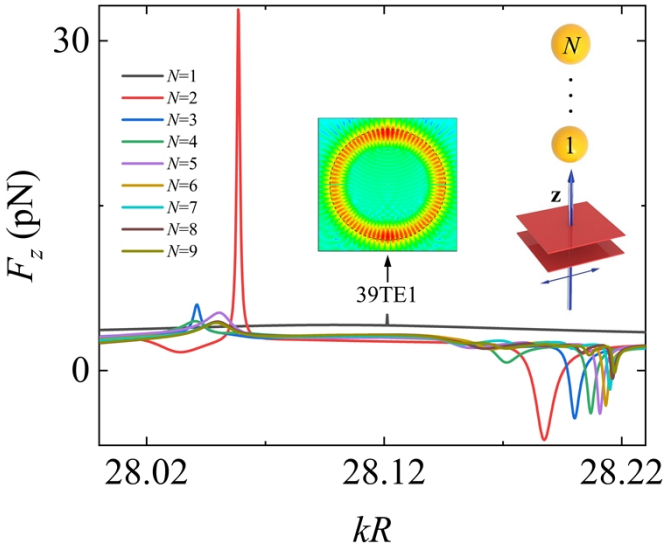

Fig. 1. The optical force exerted on the first sphere of each multiple-sphere system versus size parameter kR. The incident linearly polarized plane wave propagates along the sphere cluster's axis (z-axis) with the configuration depicted by the inset. The field distribution for the cluster composed of a single polystyrene sphere (ε = 2.5281, the outline of the sphere is denoted by the black dashed line) is also shown in the illustration beside the peak (39TE1, where 39 and 1 denote the mode and the order number [18], respectively, and TE represents transverse electric) where the WGMs is excited. The permittivity of the touching polystyrene spheres in systems with the number of spheres N = 2-9 is $\varepsilon = 2.5281 + 10^{-4}i$ [18], in which $\mathrm{Im}(\varepsilon) = 10^{-4}$ is added to obtain a reasonable Q factor considering losses due to impurities or defects in the manufacture of particles.

in Fig. 2(d), the attraction between spheres becomes complicated, which still tends to form an aggregated structure. But for the antibonding modes represented by the blue stars, the mutually repulsive optical forces drive the particles apart.

Differences between the behaviors of bonding and antibonding modes in the multiple-sphere system are further investigated by analyzing the local intensity and electric field generated on the spheres. From Figs. 3(a) and 3(c), one can see that the bonding mode has a relatively large field intensity at the contact point in the two spheres system, while the antibonding mode has the minimum field intensity. At the same time, the electric field distribution of the bonding and the antibonding modes are different near the contact point (see the enlarged electric field inset), similar to the distribution of the wave functions combined for the bonding and antibonding molecular orbitals [51], giving rise to attraction or repulsion. More importantly, we find that, for a system composed of multiple spheres, the antibonding mode is good at propagating light forward [see Figs. 3(c) and 3(d)]. The optical fields can be confined to the particle surface and continuously excited forward along the axis of the particle cluster. This can find potential applications in laser or integrated optical devices [4]. However, for the bonding mode, the maximum field intensity is always limited between the first two spheres, and the optical fields decay rapidly along the sphere cluster's axis, as seen in Figs. 3(a) and 3(b). The intensity distribution can also reflect the relative changes in the forces of the bonding and antibonding modes in Fig. 1.

Then if the system is a PT-symmetric structure composed of loss and gain spheres, what will happen to the resonance and splitting of the WGMs, and how will the corresponding optical force behave? Consider a PT-symmetric structure composed of two spheres with the refractive index

Optics EXPRESS

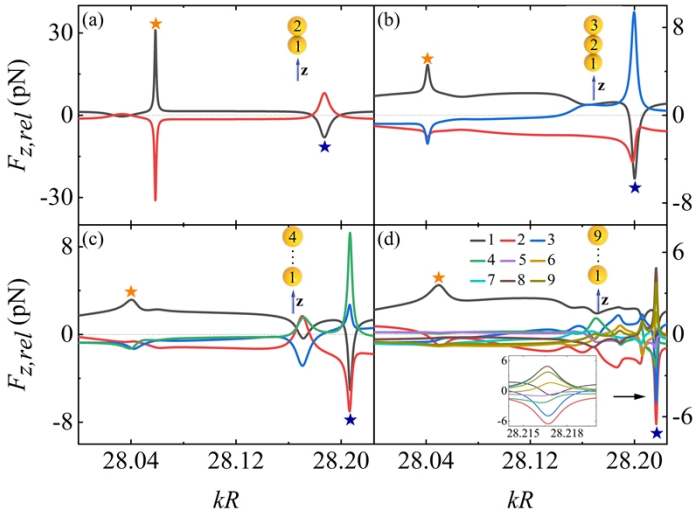

Fig. 2. Relative optical forces exerted on each sphere versus size parameter kR are shown for systems with the number of spheres $N = 2$, 3, 4, and 9, respectively [see the insert figures for the configurations and the legend of forces in (d)]. The orange and blue stars represent forces corresponding to the bonding and antibonding modes, respectively. The inset in panel (d) is an enlarged view of the peak indicated by the black arrow. The permittivity of the polystyrene spheres is $\varepsilon = 2.5281 + 10^{-4}i$.

satisfying $n(\mathbf{r}) = n^*(-\mathbf{r})$ [32–34]. It is found that for the PT-symmetric structure, their WGMs are still coherently coupled and split into the bonding and antibonding modes if the imaginary part of the refractive index is small, as seen in Fig. 4(a). And corresponding to the bonding and anti-bonding modes, there are attractive and repulsive forces between the two spheres [see Fig. 4(b)], respectively. However, with the increase of the imaginary part of the refractive index, the peaks corresponding to the bonding and antibonding modes gradually deviate from those of the lossless structure and merge progressively. From Fig. 4(a), it seems that the larger the imaginary part of the refractive index of the PT-symmetrical structure, the weak the resonance. But this is not true if one sees a more extensive range of size parameters [see Fig. 4(c), where the shade corresponds to the range of kR in Fig. 4(a)]. Strong resonances of the PT-symmetric and the lossless structures are excited over different ranges of size parameters (or frequencies).

More importantly, the total optical force of the PT-symmetric structure behaves differently from that of the lossless structure, which can be seen in Fig. 4(d). The total optical force for the structure composed of lossless materials is always positive (the black line). But for the PT-symmetric structure, no matter whether the impinging light is incident from the side of the gain sphere (the green line) or the side of the loss sphere (the magenta line), the total optical force can be negative, that is, the whole structure can move against the direction of light propagation [52–56]. And the field distributions at the peaks show the pattern of MDRs [the field intensities at the peaks corresponding to the green and magenta triangles are shown in Fig. 4(e)]. This is the same story for PT-symmetric structures composed of more spheres. However, with the further increase of the imaginary part of the refractive index, no matter whether the light is incident from the side of the gain sphere or the side of the loss sphere, the optical field is mainly distributed around the gain sphere and radiating outward [the field intensities at the peaks corresponding to the olive-green and burgundy triangles in Fig. 4(f) are shown in Fig. 4(e)]. The optical pulling force can still be obtained when the photons are mainly forward scattered, which can be clearly seen from the intensity distribution shown in Fig. 4(e). Physically, the

Optics EXPRESS

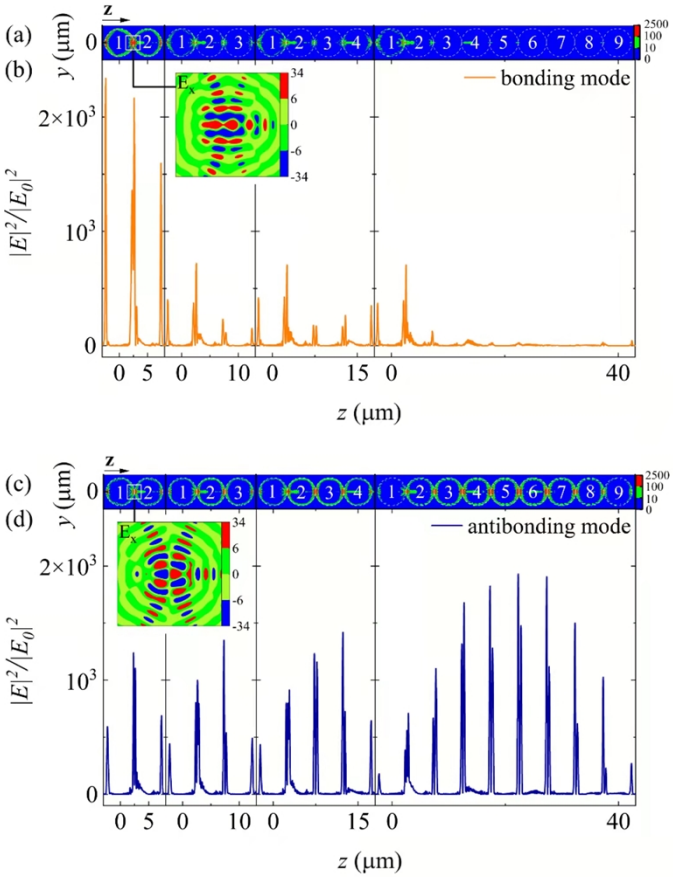

Fig. 3. (a) The intensity distribution when the bonding modes (indicated by the orange stars in Fig. 2) are excited for structures with $N = 2$, 3, 4, and 9, and the outlines of the spheres are denoted by white dotted lines. A magnified view of the x-component of the electric field on the y-z plane corresponding to the white dashed square area is shown below it. (b) The intensity distribution along the sphere cluster's axis (z-axis). (c) The intensity distribution on the y-z plane and (d) the intensity of electric fields along the sphere cluster's axis are plotted when the antibonding modes (indicated by the blue stars in Fig. 2) are excited. The permittivity of the polystyrene spheres is $\varepsilon = 2.5281 + 10^{-4}i$, and the center of the spheres are (0, 0, z) in the Cartesian coordinate system.

optical pulling force appears when the incident light has less momentum along the beam axis than the forwards-scattered photons [52]. Since the PT-symmetric structure does not have mirror symmetry, during the interaction with light, the optical force depends on the direction of the incident light, as can be seen from Figs. 4(d) and 4(f). Generally speaking, the peak positions are different when the light is incident from the side of the gain sphere or from the side of the loss sphere [40]. However, the peak positions in the lower panel of Fig. 4(d) are the same because of the relatively small imaginary part of the refractive index. If the imaginary part of the refractive index increases, such as the situation in Fig. 4(f), the vertical dashed lines show that the peak positions no longer overlap.

Optics EXPRESS

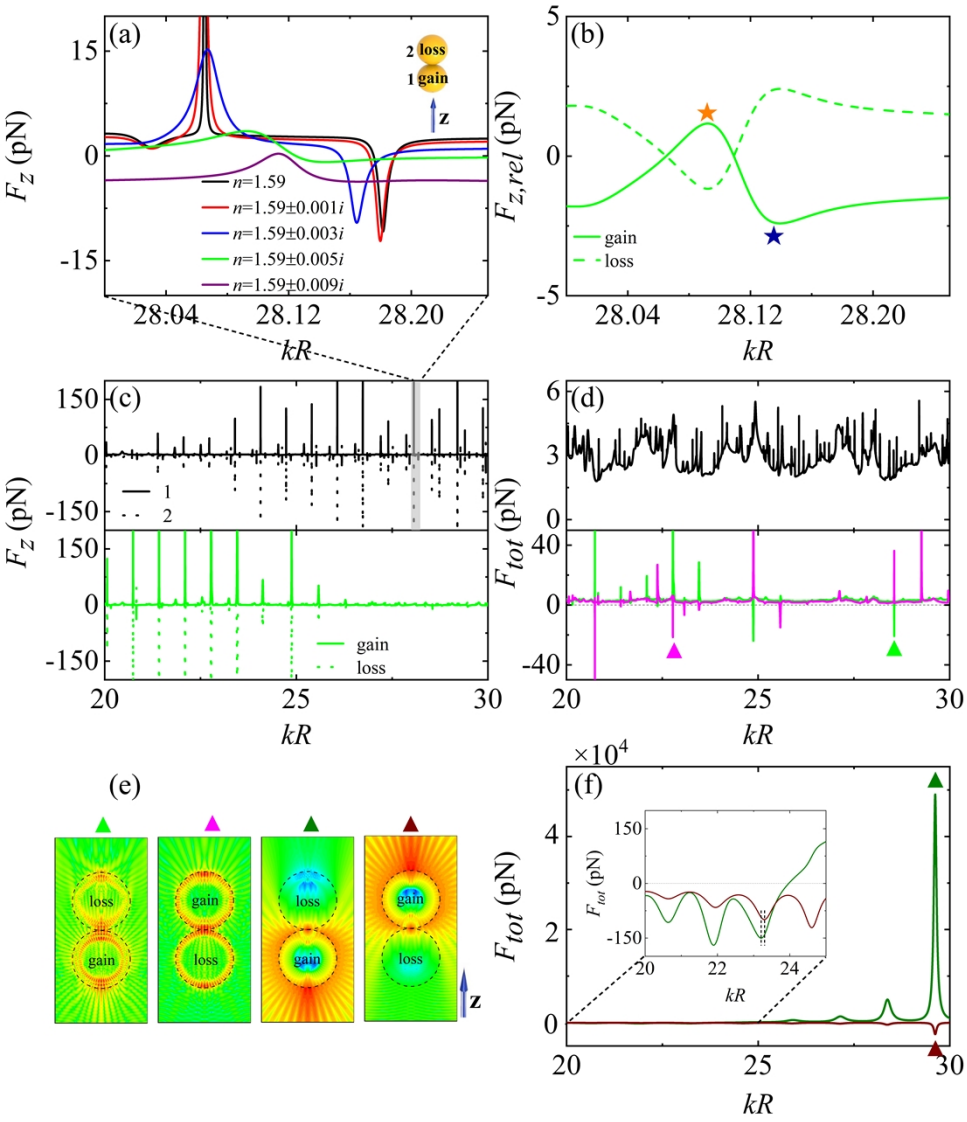

Fig. 4. (a) Optical force exerted on the first sphere of a lossless or PT-symmetric structure (see the inset) versus size parameter kR. (b) Relative optical forces exerted on each sphere in the PT-symmetric structure [see the inset in (a), $n = 1.59 \pm 0.005i$] versus kR. (c) Optical forces exerted on each sphere of a lossless (the upper panel, $n = 1.59$) or a PT-symmetric [the lower panel, see the inset in (a), $n = 1.59 \pm 0.005i$] structure versus a more extensive range of size parameters [the shade corresponds to the range of kR in (a)]. (d) The total optical force exerted on the lossless (the upper panel, $n = 1.59$) or the PT-symmetric (the lower panel, $n = 1.59 \pm 0.005i$) structure. The two cases of the incident from the side of the gain sphere or the side of the loss sphere are represented by the green and the magenta lines, respectively. The distributions of field intensities at the peaks corresponding to the green and magenta triangles are shown in (e). (f) The total optical force exerted on a PT-symmetric structure ($n = 1.59 \pm 0.136i$) with the olive-green and burgundy lines denoting the two cases of the incident from the side of the gain sphere or the side of the loss sphere, respectively. The distributions of field intensities at the peaks corresponding to olive-green and burgundy triangles are also shown in (e). The separation between adjacent spheres in PT-symmetric structure is $D = 2R + 0.01\mu$m.

Optics EXPRESS

4. Conclusion

In conclusion, the MDRs' behavior and the corresponding optical forces are investigated in a multiple-sphere system composed of a line of spheres with the same radius. The incident light used as an example is a linearly polarized plane wave propagating along the sphere cluster's axis. Other forms of incident light can also be used to investigate the resonant effect and forces. Regardless of the number of spheres in the system, their WGMs are coherently coupled and split into the bonding and antibonding modes when they approach each other. And finally, the peak positions of the bonding and antibonding modes stabilize due to the weakening coupling. Moreover, the bonding and antibonding modes all correspond to the attractive and repulsive force, respectively. More importantly, the antibonding mode is good at propagating light forward, which may find potential applications in laser or integrated optical devices. Last but not least, the bonding and antibonding modes of MDRs in the PT-symmetric system can persist only when the imaginary part of the refractive index is small enough. Furthermore, the total optical force of the PT-symmetric structure can be negative, which is completely different from that of lossless structures. Thus, the PT-symmetric structure can move towards the source at MDRs. Elaborated investigation on MDRs and resonant forces in this work provides more flexibility for optical micromanipulation.

Funding. National Natural Science Foundation of China (12174231, 12074230, 12147215); Shanxi 1331 Project; Shanxi Province Hundred Talents Project China ; Fundamental Research Program of Shanxi Province(202103021222001).

Disclosures. The authors declare no conflicts of interest.

Data availability. Data underlying the results presented in this paper are not publicly available at this time but may be obtained from the authors upon reasonable request.

References

1. S. John, "Why trap light?" Nat. Mater. **11**(12), 997–999 (2012).
2. E. N. Bulgakov and A. F. Sadreev, "Light trapping above the light cone in a one-dimensional array of dielectric spheres," Phys. Rev. A **92**(2), 023816 (2015).
3. E. N. Bulgakov and D. N. Maksimov, "Topological bound states in the continuum in arrays of dielectric spheres," Phys. Rev. Lett. **118**(26), 267401 (2017).
4. G. H. Li, T. Che, X. Q. Ji, S. D. Liu, Y. Y. Hao, Y. X. Cui, and S. Z. Liu, "Record-low-threshold lasers based on atomically smooth triangular nanoplatelet perovskite," Adv. Funct. Mater. **29**(2), 1805553 (2019).
5. L. C. Rayleigh, "The problem of the whispering gallery," Phil. Mag. **20**(120), 1001–1004 (1910).
6. C. L. Zou, C. H. Dong, J. M. Cui, F. W. Sun, Y. Yong, X. W. Wu, Z. F. Han, and G. C. Guo, "Whispering gallery mode optical microresonators fundamentals and applications," Sci. Sin-Phys. Mech. As. **42**(11), 1157–1175 (2012).
7. G. Mie, "Beiträge zur optik trüber medien,speziell kolloidaler metallösungen," Ann. Phys. **330**(3), 377–445 (1908).
8. A. Ashkin and J. M. Dziedzic, "Observation of resonances in the radiation pressure on dielectric spheres," Phys. Rev. Lett. **38**(23), 1351–1354 (1977).
9. R. E. Benner, P. W. Barber, J. F. Owen, and P. K. Chang, "Observation of structure resonances in the fluorescence spectra from microspheres," Phys. Rev. Lett. **44**(7), 475–478 (1980).
10. M. J. Jory, E. A. Perkins, and J. R. Sambles, "Light emission from whispering-gallery modes in microscopic spheres," J. Opt. Soc. Am. A **20**(9), 1785–1791 (2003).
11. Y. Y. Zhi, X. C. Yu, Q. Gong, L. Yang, and Y. F. Xiao, "Single nanoparticle detection using optical microcavities," Adv. Mater. **29**(12), 1604920 (2017).
12. Y. P. Wang, M. C. Lang, J. S. Lu, M. Q. Suo, M. C. Du, Y. B. Hou, X. H. Wang, and P. Wang, "Demonstration of intracellular real-time molecular quantification via FRET-enhanced optical microcavity," Nat. Commun. **13**(1), 1–10 (2022).
13. H. M. Dong, Y. H. Yang, and G.W. Yang, "Super low threshold plasmonic WGM lasing from an individual ZnO hexagonal microrod on an Au substrate for plasmon lasers," Sci. Rep. **5**(1), 1–7 (2015).
14. Y. E. Geints, I. V. Minin, and O. V. Minin, "Whispering-gallery modes promote enhanced optical backflow in a perforated dielectric microsphere," Opt. Lett. **47**(7), 1786–1789 (2022).
15. F. Y. Hou, Y. X. Zhan, S. F. Feng, J. S. Ye, X. K. Wang, W. F. Sun, and Y. Zhang, "Smart grating coupled whispering-gallery-mode microcavity on tip of multicore optical fiber with response enhancement," Opt. Express **30**(14), 25277–25289 (2022).
16. K. A. Fuller, "Optical resonances and two-sphere systems," Appl. Opt. **30**(33), 4716–4731 (1991).
17. M. I. Antonoyiannakis and J. B. Pendry, "Mie resonances and bonding in photonic crystals," Europhys. Lett. **40**(6), 613–618 (1997).

Optics EXPRESS

18. J. Ng, C. T. Chan, and P. Sheng, "Strong optical force induced by morphology-dependent resonances," Opt. Lett. **30**(15), 1956–1958 (2005).
19. D. B. Thompson, D. A. Keating, E. Guler, K. Ichimura, M. E. Williams, and K. A. Fuller, "Separation-sensitive measurements of morphology dependent resonances in coupled fluorescent microspheres," Opt. Express **18**(18), 19209–19218 (2010).
20. B. Vennes and T. C. Preston, "Morphology-dependent resonances in homogeneous and core-shell nonspherical particles," Phys. Rev. A **104**(3), 033512 (2021).
21. F. Han, J. A. Parker, Y. Yifat, C. Peterson, S. K. Gray, N. F. Scherer, and Z. J. Yan, "Crossover from positive to negative optical torque in mesoscale optical matter," Nat. Commun. **9**(1), 4897 (2018).
22. J. Parker, C. W. Peterson, Y. Yifat, S. A. Rice, Z. J. Yan, S. K. Gray, and N. F. Scherer, "Optical matter machines: angular momentum conversion by collective modes in optically bound nanoparticle arrays," Optica **7**(10), 1341–1348 (2020).
23. C. M. Bender and S. Boettcher, "Real spectra in non-Hermitian hamiltonians having PT-symmetry," Phys. Rev. Lett. **80**(24), 5243–5246 (1998).
24. C. M. Bender, D. C. Brody, and H. F. Jones, "Complex extension of quantum mechanics," Phys. Rev. Lett. **89**(27), 270401 (2002).
25. R. El-Ganainy, K. G. Makris, M. Khajavikhan, Z. H. Musslimani, S. Rotter, and D. N. Christodoulides, "Non-Hermitian physics and PT symmetry," Nat. Phys. **14**(1), 11–19 (2018).
26. L. Feng, Y. L. Xu, W. S. Fegadolli, M. H. Lu, J. E. B. Oliveira, V. R. Almeida, Y. F. Chen, and A. Scherer, "Experimental demonstration of a unidirectional reflectionless parity-time metamaterial at optical frequencies," Nat. Mater. **12**(2), 108–113 (2013).
27. B. Peng, Ş. K. Özdemir, F. C. Lei, F. Monifi, M. Gianfreda, G. L. Long, S. H. Fan, F. Nori, C. M. Bender, and L. Yang, "Parity-time-symmetric whispering-gallery microcavities," Nat. Phys. **10**(5), 394–398 (2014).
28. K. G. Makris, R. El-Ganainy, and D. N. Christodoulides, "Beam dynamics in PT symmetric optical lattices," Phys. Rev. Lett. **100**(10), 103904 (2008).
29. J. Luo, J. Li, and Y. Lai, "Electromagnetic impurity-immunity induced by parity-time symmetry," Phys. Rev. X **8**(3), 031035 (2018).
30. S. Longhi, "Bloch oscillations in complex crystals with PT symmetry," Phys. Rev. Lett. **103**(12), 123601 (2009).
31. W. X. Xu, S. J. Su, B. Xu, Y. W. Guo, S. L. Xu, Y. Zhao, and Y. H. Hu, "Two dimensional spacial soliton in atomic gases with PT-symmetry potential," Opt. Express **28**(23), 35297–35305 (2020).
32. R. El-Ganainy, K. G. Makris, D. N. Christodoulides, and Z. H. Musslimani, "Theory of coupled optical PT-symmetric structures," Opt. Lett. **32**(17), 2632–2634 (2007).
33. Z. Lin, H. Ramezani, T. Eichelkraut, T. Kottos, H. Cao, and D. N. Christodoulides, "Unidirectional invisibility induced by PT-symmetric periodic structures," Phys. Rev. Lett. **106**(21), 213901 (2011).
34. G. Y. Li, X. Li, L. Zhang, and J. Chen, "Gain-induced large optical torque in optical twist settings," Chin. Phys. B **29**(8), 084201 (2020).
35. C. Zhao, B. Lv, Z. Y. Pan, Z. Zhu, H. Y. Li, Z. L. Li, Y. C. Li, Y. Wang, H. Y. Mu, W. J. Li, and J. H. Shi, "Highly sensitive gas sensor based on a parity-time-symmetric system," J. Opt. Soc. Am. A **39**(2), 227–232 (2022).
36. Y. Y. Fu, Y. D. Xu, and H. Y. Chen, "Zero index metamaterials with PT symmetry in a waveguide system," Opt. Express **24**(2), 1648–1657 (2016).
37. A. Lupu, H. Benisty, and A. Degiron, "Using optical PT-symmetry for switching applications," Photonics Nanostruct. Fundam. Appl. **12**(4), 305–311 (2014).
38. H. Hodaei, M. A. Miri, M. Heinrich, D. N. Christodoulides, and M. Khajavikhan, "Parity-time-symmetric microring lasers," Science **346**(6212), 975–978 (2014).
39. R. Alaee, J. Christensen, and M. Kadic, "Optical pulling and pushing forces in bilayer PT-symmetric structures," Phys. Rev. A **9**(1), 014007 (2018).
40. R. Alaee, B. Gurlek, J. Christensen, and M. Kadic, "Optical force rectifiers based on PT-symmetric metasurfaces," Phys. Rev. B **97**(19), 195420 (2018).
41. J. Chen, K. K. Li, and X. Li, "Influence of permittivity on gradient force exerted on Mie spheres," J. Opt. Soc. Am. A **35**(4), 553–560 (2018).
42. M. Peng, H. Luo, W. Xiong, T. F. Kuang, X. L. Chen, X. Han, G. Z. Xiao, and Z. Q. Tan, "Enhanced optical trapping of ZrO2@TiO2 photonic force probe with broadened solvent compatibility," Opt. Express **30**(26), 46060–46069 (2022).
43. J. A. Stratton, *Electromagnetic theory* (McGraw-Hill, 1941).
44. C. F. Bohren and D. R. Huffman, *Absorption and scattering of light by small particles* (John Wiley and Sons, 1983).
45. Y. L. Xu, "Electromagnetic scattering by an aggregate of spheres," Appl. Opt. **34**(21), 4573–4588 (1995).
46. Y. L. Xu, "Calculation of the addition coefficients in electromagnetic multisphere scattering theory," J. Comput. Phys. **127**(2), 285–298 (1996).
47. J. Chen, J. Ng, S. Y. Liu, and Z. F. Lin, "Analytical calculation of axial optical force on a Rayleigh particle illuminated by Gaussian beams beyond the paraxial approximation," Phys. Rev. E **80**(2), 026607 (2009).
48. L. A. Ferrari and J. B. Comunale, "Splitting of low-Q Mie resonances," J. Opt. Soc. Am. A **15**(7), 1858–1866 (1998).
49. H. Miyazaki, "Ab initio tight-binding description of morphology-dependent resonance in a biosphere," Phys. Rev. B **62**(12), 7976–7997 (2000).

Optics EXPRESS

50. Y. P. Rakovich, J. F. Donegan, and M. Gerlach, "Fine structure of coupled modes in photonic molecules," Phys. Rev. A **70**(5), 051801 (2004).
51. J. Halpern, *General Chemistry: An Atoms First Approach* (Howard University, 2014).
52. J. Chen, J. Ng, Z. F. Lin, and C. T. Chan, "Optical pulling force," Nat. Photonics **5**(9), 531–534 (2011).
53. M. Peng, H. Luo, Z. J. Zhang, T. F. Kuang, D. B. Chen, W. Bai, Z. J. Chen, J. B. Yang, and G. Z. Xiao, "Optical pulling using chiral metalens as a photonic probe," Nanomaterials **11**(12), 3376 (2021).
54. N. Kostina, M. Petrov, V. Bobrovs, and A. S. Shalin, "Optical pulling and pushing forces via Bloch surface waves," Opt. Lett. **47**(18), 4592–4595 (2022).
55. H. X. Zheng, X. Li, H. J. Chen, and Z. F. Lin, "Selective transport of chiral particles by optical pulling forces," Opt. Express **29**(26), 42684–42695 (2021).
56. H. Li, Y. Y. Cao, L. M. Zhou, X. H. Xu, T. Zhu, Y. Z. Shi, C. W. Qiu, and W. Q. Ding, "Optical pulling forces and their applications," Adv. Opt. Photonics **12**(2), 288–366 (2020).